Journal of Applied Polymer Science

Structure and Properties of Aromatic Poly(benzimidazole-imide) Copolymer Fibers

Chaoqing Yin, Zixin Zhang, Jie Dong, Qinghua Zhang
State Key Laboratory for Modification of Chemical Fibers and Polymer Materials, College of Materials Science and Engineering, Donghua University, Shanghai 201620, People's Republic of China
Correspondence to: Q. Zhang (E-mail: qhzhang@dhu.edu.cn)

ABSTRACT: A series of *co*-polyimide fibers were prepared by thermal imidization of copolyamic acids derived from 3,3′,4,4′-biphenyltertracarboxylic dianhydride (BPDA) and pyromellitic dianhydride (PMDA) in various molar ratios with 2-(4-aminophenyl)−5-aminobenzimidazole (BIA). The dynamic mechanical behaviors of these polyimide (PI) fibers revealed that the glass transition temperature (T_g) was significantly improved upon increasing PMDA content. Heat-drawing process led to dramatic change on the glass transition behavior of BPDA/BIA system, but had a small impact on BPDA/PMDA/BIA *co*-polyimide fibers. This difference for PI fibers is attributed to the different degree of ordered structure of the fibers affected by heat-drawing. The incorporation of PMDA obviously improved the dimensional stability against high temperature, due to the restricted movement of polymer chains. In addition, the obtained fibers show excellent mechanical and thermal properties because of the strong hydrogen bonding due to the incorporation of benzimidazole moieties. © 2014 Wiley Periodicals, Inc. J. Appl. Polym. Sci. **2015**, *132*, 41474.

KEYWORDS: copolymers; crystallization; fibers; glass transition; polyimides

Received 15 July 2014; accepted 2 September 2014
DOI: 10.1002/app.41474

INTRODUCTION

Aromatic polyimide (PI) have been utilized in a variety of industrial fields such as electric, microelectronic, optoelectronic, and aerospace applications owing to their excellent combination of properties, including high resistance to chemicals and radiations, considerably high glass transition temperatures (T_g), low dielectric constants and good mechanical properties.[1–4] However, the properties of PI fibers are in need of further improvement when employed in severe environments. The current strong demands for PI fibers include low linear coefficients of thermal expansion (CTE), high glass transition temperature, high strength and high modulus. Upilex-S, a typical high-performance commercialized PI derived from BPDA and p-phenylenediamine (PDA), exhibits superior thermal, chemical and physical properties due to the stiff and linear chain structure, high molecular orientation and ordered structures caused by strong interchain interactions. However, the CTE value of Upilex-S ranges from 6 to 15 ppm/K depending on the film thickness and processing conditions,[5] which cannot meet some special requests.

The key strategy for reducing the CTE value is to choose PI systems consisting of rod-like backbone structures, thereby drastic chain alignment along the fiber axis can be induced during thermal imidization and heat-drawing process.[6] The rod-like PI system prepared from PMDA with a series of diamines shows a considerably low CTE (2.8 ppm/K).[7] Therefore, introducing PMDA into PI main chains is beneficial to improve corresponding dimensional stability against high temperature. Moreover, this approach brings a desirable T_g increase in many cases due to the rigid structure. Nevertheless, practically valuable low-CTE PI systems are hardly to obtain, because such rod-like PI systems may result in brittle fibers owing to poor chain entanglement.

To reduce the CTE value and maintain the thermal and mechanical properties of PI fibers in the meantime, one attempted approach is structural modification. So far, many efforts on chemical modification of PI structures have been done, including the introduction of heterocyclic rings like both benzoxazole and benxadiazole,[8,9] pyridine,[10–12] pyrimidine,[13,14] furan,[15,16]and phthalazinone[17] in polymer backbone, which led to good thermal and mechanical properties of these PIs. Polybenzimidazoles (PBIs) are another class of high-performance polymer that containing recurrent benzimidazole rings, which have been used extensively in the aerospace industry recent years due to their high-strength, high-modulus and sufficient thermal stability to withstand extreme conditions.[18–20] In the view of the desirable properties of PIs and PBIs, the incorporation of benzimidazole moieties into the PI main chains is

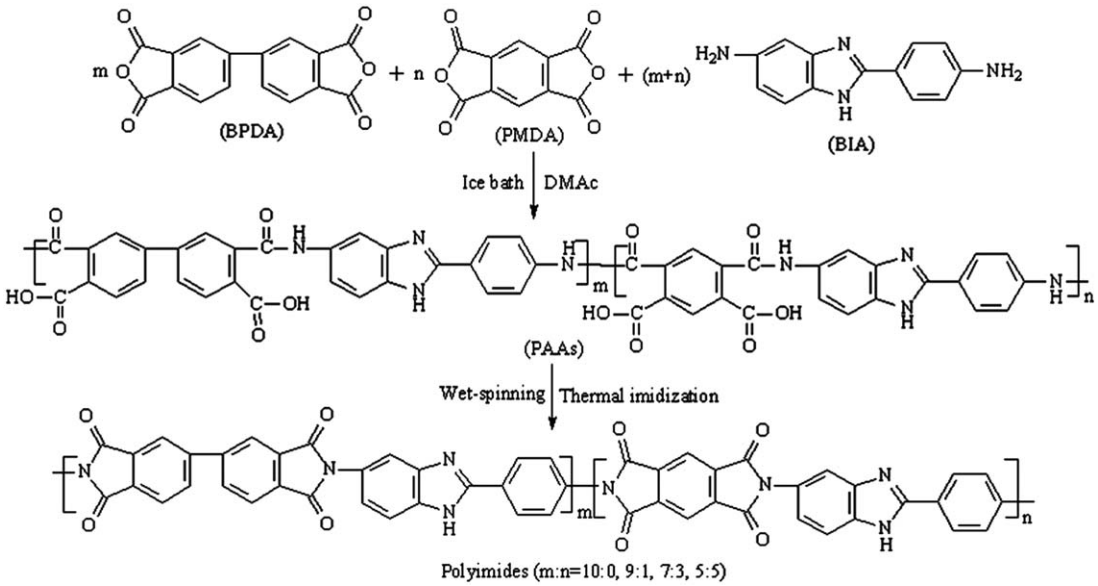

Scheme 1. Synthesis of PIs (BPDA/PMDA/BIA) and fiber preparation.

expected to improve the thermal and mechanical properties. Taking the above-mentioned factors into consideration, we hypothesize that the combination of BPDA, PMDA, and benzimidazole moieties in the backbone of PIs would be the right track to meet the integrated performance requirements for severer environments.

In this study, a series of *co*-polyimide fibers were fabricated from BIA and two dianhydrides, BPDA, and PMDA. We focus here on the dynamic mechanical properties, molecular packing and dimensional stability of the obtained fibers, and in addition, the thermal and mechanical properties of *co*-polyimide fibers were also investigated in detail.

EXPERIMENTAL

Materials

N,N-dimethylacetamide (DMAc) with a trace of water < 100 ppm was provided by Shanghai Jinshan Jingwei Chemical. Pyromellitic dianhydride (PMDA) was obtained from Shanghai Synthetic Resin Research Institute, and 3,3',4,4'-biphenyltertracarboxylic dianhydride (BPDA) was obtained from Shijiazhuang Haili Fine-Chemical. 2-(4-Aminophenyl)−5-aminobenzimidazole (BIA) was purchased from Changzhou Sunlight Pharmaceutical. Distilled water and other materials were used as received.

Synthesis of Polyamic Acid Solutions

The polyamic acid (PAA) solution with a solid content of 13.5 wt % was prepared through a typical synthetic route.[21] For the polymerization, the molar ratios of the two dianhydrides (BPDA : PMDA) were 10 : 0, 9 : 1, 7 : 3, and 5 : 5, denoted as homo-PAA, *co*-PAA-1, *co*-PAA-2, and *co*-PAA-3.

Preparation of Polyimide Fibers

Wet spinning was employed to prepare PAA fibers with a self-built experimental spinning machine. Homogeneous PAA solution was extruded through a spinneret of 50 holes with a diameter of 0.08 mm, and then entered into a coagulation bath at room temperature, which contains a mixture of water/DMAc in the ratio of 5 : 5 (v/v). The solidified fibers were washed thoroughly with distilled water to remove residual DMAc, and dried in vacuum oven for 20 h at 60°C. PI fibers were produced via thermal imidization of precursor fibers under vacuum at 80, 140, 220, and 300°C each for 1 h, followed by drawing process with various ratios in a furnace over 450°C. Scheme 1 shows the synthetic process and the chemical structure of the PIs.

Measurements

Two-dimensional wide angle X-ray diffraction (2D WAXD) profiles were obtained at Beamline (16B1) in Shanghai Synchrotron Radiation Facility (SSRF). The wavelength used was 1.24Å. A CCD X-ray detector (MAR CCD 165) was employed at distances of 79.54 and 5060 mm from the sample for WAXD and SAXS measurements, respectively. In all patterns, the fiber axes

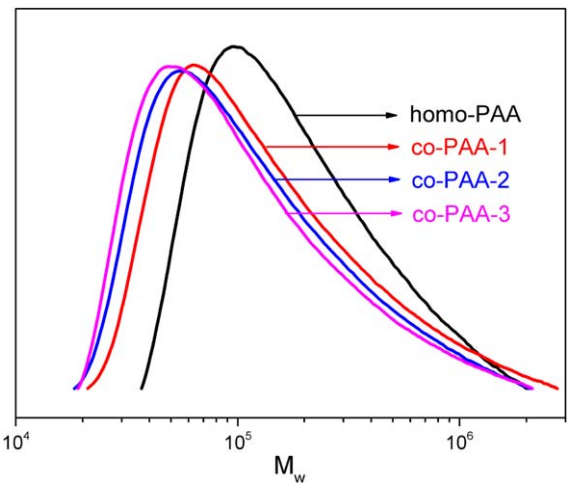

Figure 1. Molecular weight distribution curves of PAA solutions. [Color figure can be viewed in the online issue, which is available at wileyonlinelibrary.com.]

Table I. Molecular Weights and PDIs of PAAs

Samples	Molar ratio (BPDA/PMDA)	M_n ($\times 10^4$)	M_w ($\times 10^5$)	PDI
Homo-PAA	10 : 0	8.83	2.63	2.9
co-PAA-1	9 : 1	7.67	3.00	3.9
co-PAA-2	7 : 3	7.55	2.17	2.9
co-PAA-3	5 : 5	7.37	2.26	3.1

are oriented vertically. The 2D WAXD pattern was processed with the software package x-Polar to correct for air scattering. The corresponding profiles were normalized to beam intensity and corrected relative to an empty sample cell background. A typical image acquisition time was 40 s. The images were carried out using the software package x-Polar.

The molecular weights of PAAs were determined by gel permeation chromatography (GPC) analyses with DMAc as eluant at 40°C. Fiber density measurements were performed using an SVM3000 machine (Anton Paar GmbH). The linear CTE and dynamic mechanical analysis (DMA) of fibers were performed on a TA instrument Q800 under N_2 atmosphere at a heating rate of 10 and 5°C/min, respectively. Fourier Transform Infrared (FTIR) spectra of the PAA and PI fibers were obtained with a Nicolet 8700 spectroscope with the range of 4000–400 cm^{-1}. Thermogravimetric analysis (TGA) was carried with a Discovery TGA Q5000IR under nitrogen flow at a heating rate of 10°C/min. The mechanical properties of PI fibers were measured using an XQ-1 tensile testing machine at a drawing rate of 10 mm/min with a gauge length of 20 mm.

RESULTS AND DISCUSSION

The Molecular Weight of PAAs

As we know, the initial molecular weight of PAAs has a great influence on the final performance of PI fibers. Figure 1 shows the GPC spectra of PAAs with various dianhydride ratios, and the detail values of the molecular weight and polydispersity index (PDI) are shown in Table I. The synthesized PAAs have relatively high molecular weights, which is very important for the preparation of high-performance PI fibers. In Table I, the homo-PAA from BPDA/BIA system has a relatively higher molecular weight and narrower molecular distribution than those of BPDA/PMDA/BIA copolymer systems. Namely, the addition of PMDA has a negative effect on the molecular weight and PDI of the PAAs, which may be attributed to the difference of the electron-withdrawing ability between PMDA and BPDA.

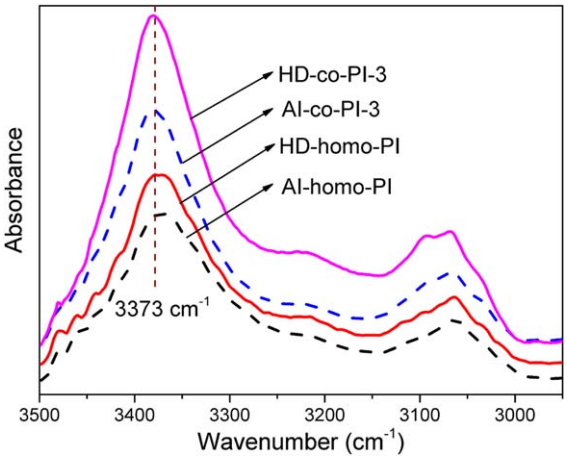

Figure 3. ATR-FTIR spectra of the as-imidized and heat-drawn PI fibers with various dianhydride ratios. [Color figure can be viewed in the online issue, which is available at wileyonlinelibrary.com.]

The Effect of Heat-Drawing on the Dynamic Mechanical Properties of PI Fibers

Figure 2 shows the effect of heat-drawing on the dynamic mechanical properties of PI fibers. For homo-(BPDA/BIA) PI fiber, there exists drastic changes in the storage modulus (E') and tan δ curves after the heat-drawing process. The E' decreases much more gradually at T_g, and the peak value of tan δ obviously reduces [Figure 2(a)]. On the other hand, the heat-drawn *co*-PI-3 fiber exhibited similar E' and tan δ tendency as the fiber annealed at 300°C [Figure 2(b)], except for a slight T_g increase of ca. 10°C.

The change of glass transition behavior of the PI fibers may be attributed to the intensification of the interchain interactions in the amorphous region and the increase of the crystal fraction. The former includes hydrogen bonding interaction[22] and charge-transfer complex[23] like physical cross-links. We have tried to observe the fluorescence spectra of all PI fibers, nevertheless, all of the samples only exhibited extremely indistinct peaks at ~590 nm (not shown here), suggesting a weak charge-

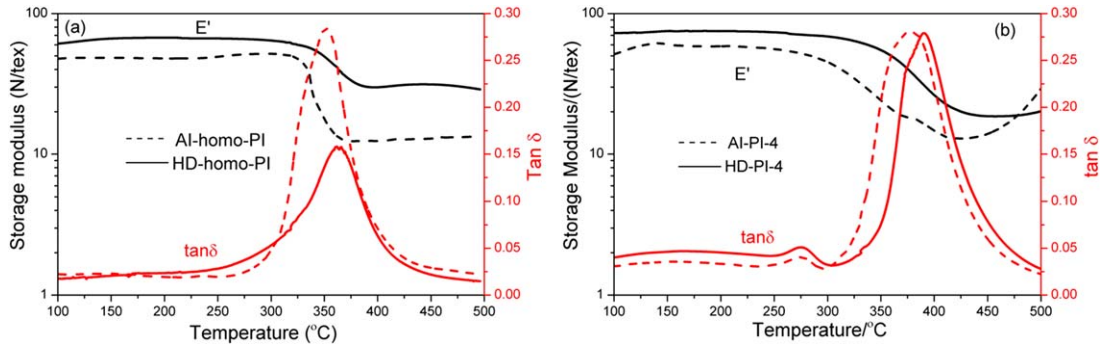

Figure 2. E' and tan δ curves for (a) homo-PI and (b) *co*-PI-3 fibers, including both as-imidized (AI) and heat-drawn (HD) fibers. [Color figure can be viewed in the online issue, which is available at wileyonlinelibrary.com.]

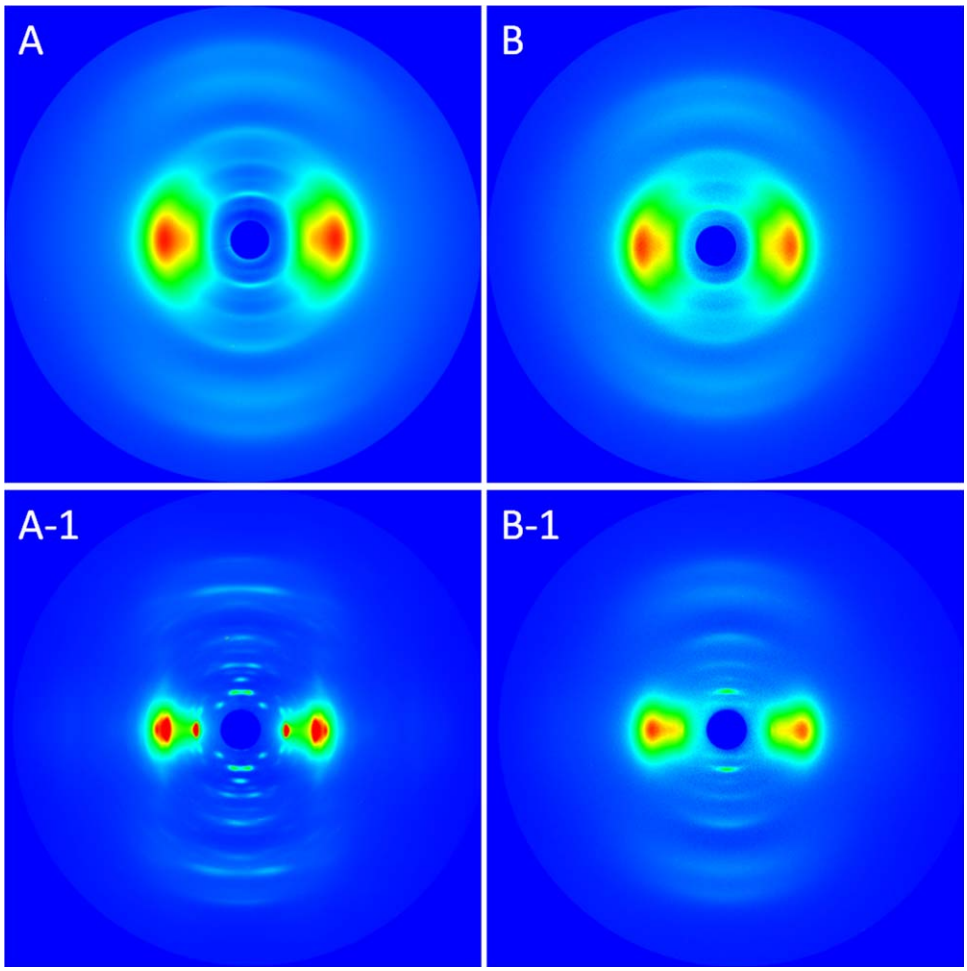

Figure 4. 2D WAXD patterns of the PI fibers: (A) AI-homo-PI, (A-1) HD-homo-PI, (B) AI-*co*-PI-3, and (B-1) HD-*co*-PI-3. [Color figure can be viewed in the online issue, which is available at wileyonlinelibrary.com.]

transfer complex. Meanwhile, the hydrogen bonding interaction has been considered to be the strongest physical interaction, which can be detected via FTIR. The FTIR spectra of the four samples are shown in Figure 3. In the region of 3500–2950 cm^{-1}, the stretching bands of N—H groups are observed at about 3373 cm^{-1} for all the fibers. According to the previous works, the existence of the hydrogen bonding interaction would make a great effect on the frequency shifts of the functional groups. However, in our case, there is no distinctive difference on the frequency of N—H band for the four fibers, which implies that hydrogen bonding interaction hasn't changed by the incorporation of PMDA units.

It is well known that the aggregation structure is of great importance on the dynamical behavior of the fibers. Figure 4 displays the 2D WAXD patterns of homo-PI and *co*-PI-3 fibers before and after heat-drawing. Figure 4(A,B) of as-imidized fibers exhibit diffused diffraction streaks along both equatorial and meridian directions, indicating a typical amorphous structure.

On the equator, no obvious changes occur after heat-drawing for *co*-PI-3 fiber, as shown in Figure 4B. In contrast, for the homo-(BPDA/BIA) fiber, the sign of crystallization in the patterns becomes prominent after heat-drawing, where two discernible peaks at $2\theta = 10.4$ and 16.8° with *d*-spacing values of 6.8 and 4.2Å can be observed on the equator, respectively, representing a highly ordered arrangement of the molecular chains [Figure 5(A)]. The former peak (10.4°) in the small angle region is sharp and intensive, whereas the later one (16.8°) in the larger angle region is quite weak and broad, suggesting that the homo-PI fiber does not exhibit definitive crystalline structures. The calculated *d*-spacing of the peaks at 16.8° (4.2Å) is close to the distance on (110) diffraction planes between two neighboring rod-like molecular chains of monomethyl-pendant poly(p-phenylene benzobisimidazole) (MePBI), respectively.[24,25]

In the meridian region, substantial changes are observed for homo-PI fibers after heat-drawing, as shown in Figure 5(A-1). Besides, the reflection of BPDA/BIA system appeared as narrow meridianal arcs, indicating a highly ordered structure along the fiber axis, while the arcs of patterns in *co*-PI-3 fibers are longer and more diffused. Six Bragg diffraction streaks, related to the periodicity along the polymer chains, at $2\theta = 8.8$ (with strong intensity), 11.6 (medium), 13.3 (weak), 14.9 (medium), 20.5 (medium), and 29.8° can be observed [Figure 5(A-1)] for heat-drawn homo-PI fibers. Furthermore, there are obvious

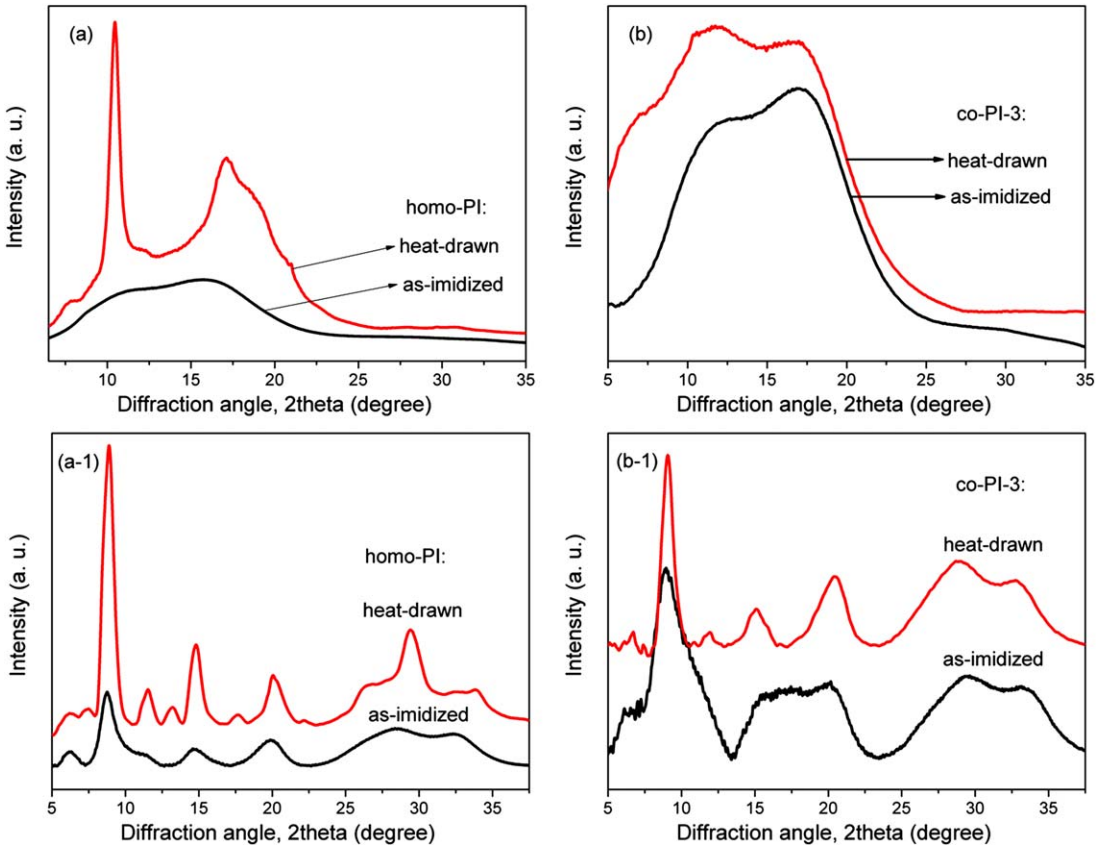

Figure 5. 1D WAXD patterns of PI fibers: (A) and (B) equator; (A-1) and (B-1) meridian directions. [Color figure can be viewed in the online issue, which is available at wileyonlinelibrary.com.]

diffractions in the quadrants, which illustrate the existence of 3D crystalline structures. On the other hand, in *co*-PI-3 fibers, although a few new small peaks occurs via heat treatment, the peaks are more diffused and less intensive, compared with that of homo-PI fibers. Therefore, we can conclude that the prepared homo-(BPDA/BIA) fiber has a well-defined ordered crystal structure, while the macromolecular structure of *co*-PI-3 fibers are less ordered.

The regularity of molecular structures decreases mainly owing to the increase of PMDA/BIA units, which are randomly distributed in the BPDA/BIA segments. The results demonstrate that the introduction of rigid PMDA destroys the stress induced crystallization behavior of PI fibers, which explains why heat-drawing results in different dynamic mechanical properties of PI and *co*-PI fibers.

The reduced regularity upon PMDA content of *co*-polyimide fibers is not consistent with the general consideration of introducing rigid PMDA. The decreased ordered structure of *co*-PI fiber can be partially explained in terms of the long range conformation of polymer chains. As BPDA possesses one more rotatable bond than PMDA, the flexibility of the polymer chains obviously decreases after replacing some of the BPDA/BIA units with the PMDA/BIA. Figure 6 schematically depicts the profiles of the lowest energy conformation for homo-(BPDA/BIA), homo-(PMDA/BIA), and *co*-(BPDA/PMDA/BIA) tetramers, molecular modeling of the structures is conducted on the Material Studio software. Obviously, biphenyl or phenylbenzimidazole groups in BPDA/BIA segments are liable to take the coplanar state, while PMDA/BIA cannot take the coplanar form owing to the inherent rigidity of PMDA. We can expect that in the BTDA-BIA units are preferred to build regularly stacking regions in *co*-PI fibers. The introduction of the PMDA causes an increase in the content of conformational defects and consequently to a reduction of molecular regularity, which is consistent with the WAXD results (Figures 4 and 5).

Density measurements of the PI fibers are employed to further investigate the molecular packing. As shown in Table II, the density values range from 1.404 to 1.459 g/cm^3. Obviously, heat-drawing significantly enhances the density of homo-PI, while the densities of the *co*-PI fibers only increase slightly. The results suggest that BPDA/BIA fiber can take a higher degree of molecular packing via heat-drawing process, but those containing PMDA cannot. The density results correspond well to the effect of heat-drawing on the WAXD, E' and tan δ curves for PI fibers.

Dynamic Mechanical Properties and Linear CTE of PI Fibers

Considering the difference of the rigidity and aggregation structure between the homo-BPDA/BIA and *co*-PI fibers containing PMDA units, we expect a substantial enhancement in storage modulus (E') and other thermal dynamical properties of the PI fibers. Figure 7 displays tan δ and the dynamic storage modulus (E') as a function of temperature for heat-drawn PI fibers.

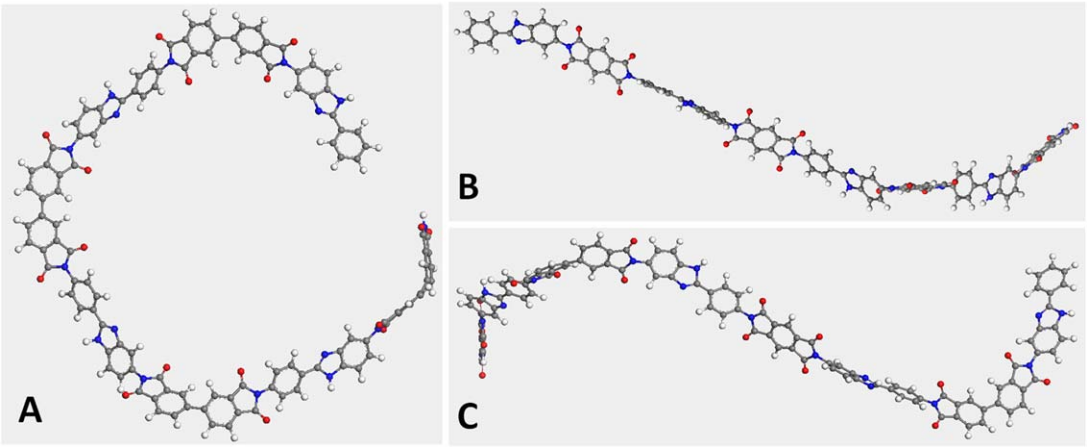

Figure 6. Schematic diagram for the conformation of homo-PI tetramers: (A) BPDA/BIA, (B) PMDA/BIA, and (C) copoly (BPDA/PMDA/BIA). [Color figure can be viewed in the online issue, which is available at wileyonlinelibrary.com.]

The glass transition temperature T_g (peak temperature of tan δ) of the heat-drawn fibers displays an obviously increasing trend upon increasing PMDA content. The semirigid BPDA/BIA fiber exhibits a T_g at 361°C; by introducing the PMDA into the BPDA/BIA segments, the T_g values of *co*-PI-1, *co*-PI-2, and *co*-PI-3 are 364, 377, and 389°C, respectively, indicating that thermal resistance is significantly improved with increasing PMDA content. An explanation on the higher T_g of *co*-PI-3 fiber may be that the coplanar rotation or cooperative conformational change is more restricted, as illustrated by the molecular modeling of homo-PI tetramers (Figure 6). Besides, it should be noted that *co*-PI-2 (269 and 377°C) and *co*-PI-3 (276 and 389°C) fibers exhibit two α relaxation peaks, which are ascribed to glass transitions on the basis of activation energies in the mobile amorphous regions of the materials. The appearance of a small peak at lower temperature indicates a separate glass transition of chain segments. This further demonstrates a considerable but not completely homogeneous phase of BPDA/PMDA/BIA copolymer systems.[26] The occurrence of two glass transition temperatures for these copolymers may be attributed to the two reasons: (a) random and block copolymerization coexist in the polymers,[27] (b) the broader distribution of molecular weight upon PMDA content.[28] The first T_g occurring at low temperature may be attributed to a low-molecular segment rich phase and the one appearing at higher temperature can be attributed to high-molecular segment rich phase.[28] The dynamic storage modulus (E') of PI fibers with various PMDA contents is shown in Figure 7(b). The E' of the fibers slightly increases upon increasing PMDA content below glass transition temperature. For homo-(BPDA/BIA) fiber, E' decreases at the T_g more gradually than that for *co*-polyimide fibers, this is often observed in highly cross-linked or highly crystallized polymers. It is understandable that the semirigid segments of BPDA/BIA induce strong interchain interactions and consequently forms crystal-like order, as illustrated by WAXD patterns (Figure 4).

Table II. Density Values of the Polyimide Fibers

Density (g/cm^3)	homo-PI	*co*-PI-1	*co*-PI-2	*co*-PI-3
As-imidized	1.416	1.408	1.409	1.404
Heat-drawn	1.459	1.417	1.415	1.411

Although molecular mobility of semirigid PI chains like BPDA/PMDA/BIA is recognized to be significantly restricted, molecular motions can be allowed during heat-drawing of PI fibers as a sort of "molecular motion-controlled" process. Therefore, for PI fibers, heat-drawing above the T_g often favorably acts for a significant morphological change due to chain rearrangement, which further affects the dimensional stability of fibers.

Figure 8 displays the influence of PMDA on CTE for as-imidized and heat-drawn PI fibers, which all exhibit negative values. As can be seen a pronounced PMDA content dependence is observed in both AI-PI and HD-PI fibers, the dimensional stability are appreciably improved after the incorporation of PMDA. For as-imidized fibers, the CTE values of homo-PI, *co*-PI-1, *co*-PI-2, and *co*-PI-3 are −11.3, −9.9, −8.1, and −6.5 ppm/K, respectively. It should be noted that the magnitude (−6.5 ppm/K) is comparable with the value in the stretching direction of a uniaxially oriented PBO fiber with an ultimately high Hermann's orientation function >0.99, i.e., CTE = −6 ppm/K for Zylon HM type.[29] On the other hand, the heat-drawing contributes to drastic enhancement of CTE values for BPDA/PMDA/BIA fibers, as illustrated by the fact that heat-drawing induces high level of orientation of PI fibers. For the HD-*co*-PI-1, HD-*co*-PI-2, and HD-*co*-PI-3 fibers, the CTE values are −7.7, −6.0, −4.3 ppm/K, respectively, while this value for BPDA/BIA system reaches to −8.8 ppm/K. As a comparison, the CTE value of BPDA/2,2'-bis(trifluoromethyl)−4,4'-diaminobiphenyl (PFMB) PI fiber is −5.0 ppm/K at a stress of 6 MPa,[30] and that of Kevlar 49 is −8.3 ppm/K at a load of 200 N.[31] Therefore, the incorporation of PMDA in the main chains leads to a good dimension stability of the *co*-polyimide fibers, attributing to the highly restricted movement of rod-like PMDA. The result amply demonstrates that the fibers consisting of rod-like backbone structure tend to exhibit superior dimensional stability. The typical plots of shrinkage strain as a function of temperature at the stress of 8 MPa are presented in Figure 9.

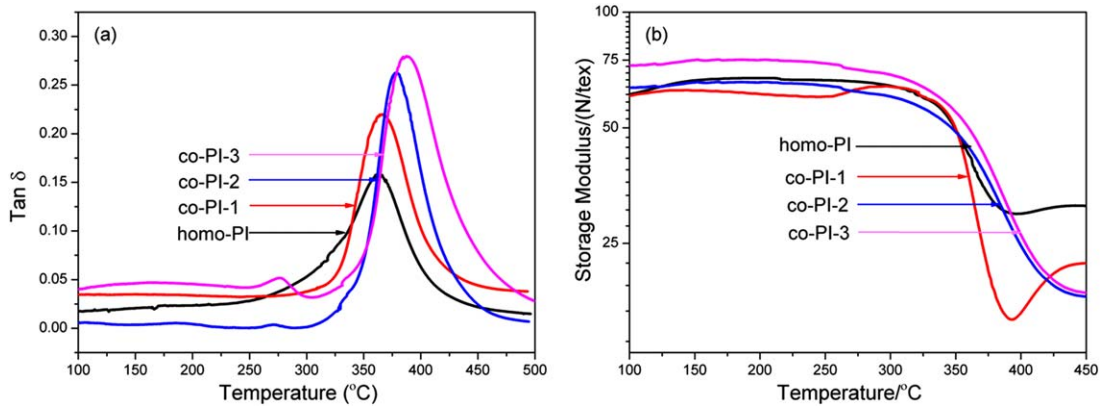

Figure 7. Tan δ (a) and dynamic storage modulus (E') (b) as a function of temperature for heat-drawn PI fibers with various dianhydride ratios. [Color figure can be viewed in the online issue, which is available at wileyonlinelibrary.com.]

Properties of PI Fibers

The solubility of the obtained PI fibers was tested in various polar aprotic solvents including DMAc, *N*,*N*-Dimethylformamide (DMF), *N*-methyl-2-pyrrolidone (NMP), dimethyl sulfoxide (DMSO), and phenolic solvents such as m-cresol. It turns out that none of the PI fibers is soluble in the above solvents even at 70°C, indicating that BPDA/PMDA/BIA polyimide exhibits excellent chemical resistance.

Mechanical properties of the PI fibers are summarized in Table III. The prepared fibers exhibit a tensile strength of 1.32-1.43 GPa and an initial modulus of 52.9–69.5 GPa, indicating the exceptional performance of PI fibers. The tensile strength and elongation at break gradually decrease with increasing PMDA content, while the initial modulus significantly increases. The elongation at break of *co*-PI-3 fiber is 1.9%, which is much lower than that of homo-PI fiber, with the value of 2.7%.

Slight reduced mechanical performance of the *co*-polyimide fibers containing PMDA is further clarified. The mechanical properties depend mainly on the molecular weight, chain structure and aggregation structure of macromolecules. Generally, better mechanical properties of the polymers are probably obtained with higher molecular weight, crystallinity or macromolecular orientation. As shown in Table I, the molecular weight of PAA solutions decreased slightly after introducing PMDA, which implies that the deterioration of mechanical properties is partially affected by the molecular weight. Besides, the introduction of PMDA plays a negative role on the crystalline properties of *co*-polyimide fibers, as described in WAXD (Figure 4). Therefore, the deterioration of the mechanical properties of the *co*-polyimide fibers containing PMDA can be

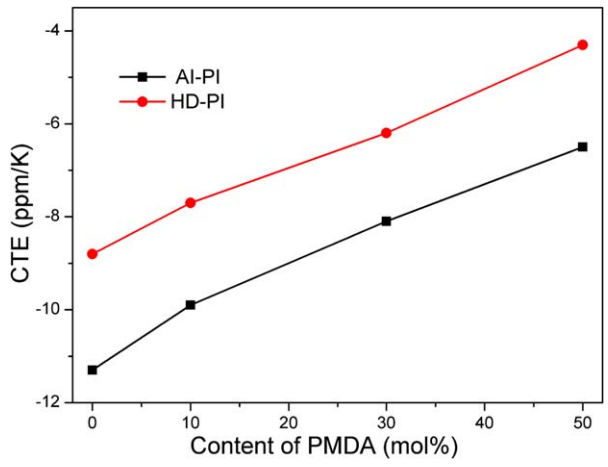

Figure 8. Influence of PMDA content on CTE for as-imidized and heat-drawn PI fibers. [Color figure can be viewed in the online issue, which is available at wileyonlinelibrary.com.]

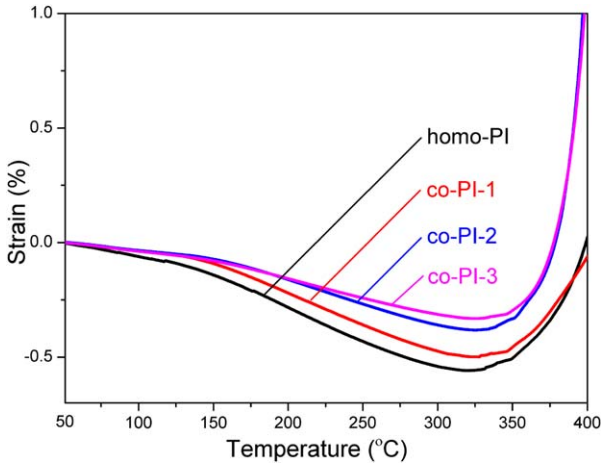

Figure 9. Plots of shrinkage strain vs. temperature for the heat-drawn fibers at a stress of 8 MPa. [Color figure can be viewed in the online issue, which is available at wileyonlinelibrary.com.]

Table III. Mechanical Properties of Heat-Drawn Polyimide Fibers

Sample	Tensile strength (GPa)	Initial modulus (GPa)	Elongation at break (%)
homo-PI	1.43 ± 0.10	52.9 ± 5.1	2.7 ± 0.21
co-PI-1	1.37 ± 0.10	57.1 ± 5.3	2.4 ± 0.22
co-PI-2	1.36 ± 0.10	61.8 ± 5.4	2.2 ± 0.19
co-PI-3	1.32 ± 0.11	69.5 ± 6.1	1.9 ± 0.20

Table IV. Thermal Properties of the Polyimide Fibers

Samples	T_g (°C)	T_d (°C)	T_p (°C)	Char yield (wt %)
homo-PI	361	617	643	74.0
co-PI-1	364	614	642	72.7
co-PI-2	269, 377	610	628	72.2
co-PI-3	276, 389	605	635	71.7

attributed to the relatively lower molecular weight and the decrease of the ordered degree of the copolymers.

Moreover, TGA was employed to investigate the thermal properties of the PI fibers, as shown in Table IV and Figure 10. The char yields at 750°C in nitrogen are higher than 70%, 5% weight loss temperatures (T_d) are observed in the range of 605–617°C, and the maximum degradation rate of PI fibers occurs at the temperature of 635–643°C (T_p). The different thermal stability above is related to the polymer compositions and structures. The thermal stability of the *co*-polyimide fibers slightly decreases along with elevated PMDA content.

CONCLUSIONS

Heat-drawing has a marked influence on the E' and tan δ curves of as-imidized BPDA/BIA homo-polyimide fibers but affects little on those of the *co*-polyimide fibers, as the introduction of PMDA destroys the stress inducing crystal-like formation of PI fibers. The abrupt E' decrease at the T_g for the fibers containing PMDA was related to less ordered structure of the fibers owing to the non-coplanar conformation. Upon increasing PMDA content, the glass transition temperature of PI fibers significantly is enhanced, indicating an improved thermal resistance. PI fibers shown a lower linear coefficient of thermal expansion by incorporating PMDA units into the polymer chains, due to the restricted macromolecular movement. Though the addition of PMDA slightly decreases the mechanical properties of PI fibers, the corresponding dynamic mechanical properties and dimensional stability are dramatically enhanced.

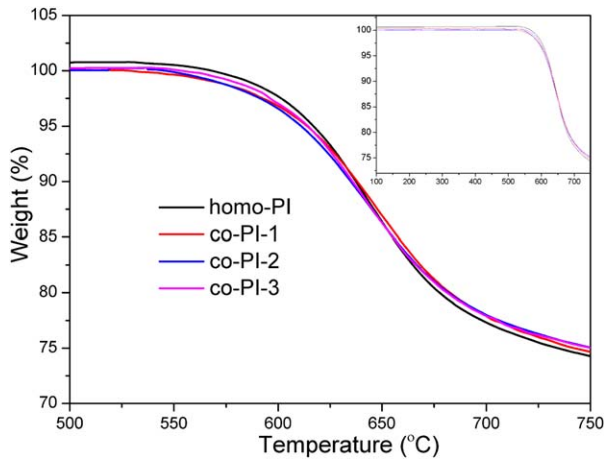

Figure 10. TGA curves of the PI fibers. [Color figure can be viewed in the online issue, which is available at wileyonlinelibrary.com.]

ACKNOWLEDGMENTS

Financial support of this work is provided by NSFC (51233001, 51173024), 973 Plan (2014CB643603), 111 Project (111-2-04) and Chinese Universities Scientific Fund (14D310602). 2D WAXD experiments were performed at 16B1 Beamline station in Shanghai Synchrotron Radiation Facility (SSRF).

REFERENCES

1. Liu, J.; Zhang, Q.; Xia, Q.; Dong, J.; Xu, Q. *Polym. Degrad. Stab.* **2012**, *97*, 987.
2. Zhang, Q. H.; Dai, M.; Ding, M. X.; Chen, D.; Gao, L. X. *Eur. Polym. J.* **2004**, *40*, 2487.
3. Afshari, M.; Sikkema, D. J.; Lee, K.; Bogle, M. *Polym. Rev.* **2008**, *48*, 230.
4. Eashoo, M.; Wu, Z. Q.; Zhang, A. Q.; Shen, D. X.; Tse, C.; Harris, F. W.; Cheng, S. Z. D.; Gardner, K. H.; Hsiao, B. S. *Macromol. Chem. Phys.* **1994**, *195*, 2207.
5. Ishii, J.; Takata, A.; Oami, Y.; Yokota, R.; Vladimirov, L.; Hasegawa, M. *Eur. Polym. J.* **2010**, *46*, 681.
6. Ebisawa, S.; Ishii, J.; Sato, M.; Vladimirov, L.; Hasegawa, M. *Eur. Polym. J.* **2010**, *46*, 283.
7. Sensui, N.; Ishii, J.; Takata, A.; Oami, Y.; Hasegawa, M.; Yokota, R. *High. Perform. Polym.* **2009**, *21*, 709.
8. Kayukova, L. A.; Beketov, K. M.; Akhelova, A. L.; Praliev, K. D. *Khim. Geterotsikl. Soenin.* **2006**, 1057.
9. Murugan, V.; Prasad, K. R.; Sarma, G. V. S. R.; Ramanathan, M.; Suresh, B. *Ind. J. Heterocycl. Chem.* **2001**, *11*, 169.
10. Aram, E.; Mehdipour-Ataei, S. *J. Appl. Polym. Sci.* **2013**, *128*, 4387.
11. Seyedjamali, H.; Pirisedigh, A. *Polym. Bull.* **2012**, *68*, 299.
12. Lei, R.; Kang, C. Q.; Huang, Y. J.; Li, Y. H.; Wang, X.; Jin, R. Z.; Qiu, X. P.; Ji, X. L.; Xing, W.; Gao, L. X. *J. Appl. Polym. Sci.* **2009**, *114*, 3190.
13. Garmonova, T. I.; Artemeva, V. N.; Nekrasova, Y. M. *Vysokomol. Soedin. Ser. A* **1990**, *32*, 2062.
14. Xia, A. X.; Lu, G. H.; Qiu, X. P.; Guo, H. Q.; Zhao, J. Y.; Ding, M. X.; Gao, L. X. *J. Appl. Polym. Sci.* **2006**, *102*, 5871.
15. Banihashemi, A.; Abdolmaleki, A. *Eur. Polym. J.* **2004**, *40*, 1629.
16. Matsumoto, T.; Nishimura, K.; Kurosaki, T. *Eur. Polym. J.* **1999**, *35*, 1529.
17. Wang, J. Y.; Liao, G. X.; Liu, C.; Jian, X. G. J. Polym. Sci., *Part A: Polym. Chem.* **2004**, *42*, 6089.
18. Qian, G. Q.; Benicewicz, B. C. *J. Polym. Sci., Part A: Polym. Chem.* **2009**, *47*, 4064.
19. Banihashemi, A.; Atabaki, F. *Eur. Polym. J.* **2002**, *38*, 2119.
20. Wang, H. H.; Wu, S. P. *J. Appl. Polym. Sci.* **2003**, *90*, 1435.
21. Xia, Q. M.; Liu, J. P.; Dong, J.; Yin, C. Q.; Du, Y. X.; Xu, Q.; Zhang, Q. H. *J. Appl. Polym. Sci.* **2013**, *129*, 145.
22. Luo, L. B.; Pang, Y. W.; Jiang, X.; Wang, X.; Zhang, P.; Chen, Y.; Peng, C. R.; Liu, X. Y. *J. Polym. Res.* **2012**, *19*, 9783.

23. Hasegawa, M.; Kochi, M.; Mita, I.; Yokota, R. *Eur. Polym. J.* **1989**, *25*, 349.
24. Jenkins, S.; Jacob, K. I.; Polk, M. B.; Kumar, S.; Dang, T. D.; Arnold, F. E. *Macromolecules* **2000**, *33*, 8731.
25. Wakita, J.; Jin, S.; Shin, T. J.; Ree, M.; Ando, S. *Macromolecules* **2010**, *43*, 1930.
26. Auschra, C.; Stadler, R. *Macromolecules* **1993**, *26*, 6364.
27. Kuo, S. W.; Tsai, H. T. *J. Appl. Polym. Sci.* **2012**, *123*, 3275.
28. Schranz, W.; Reinecker, M.; Soprunyuk, V.; Fally, M.; Sanchez-Ferrer, A. *Soft Matter* **2014**, *10*, 5729.
29. Kitagawa, T.; Murase, H.; Yabuki, K. *J. Polym. Sci., Part B: Polym. Phys.* **1998**, *36*, 39.
30. Eashoo, M.; Shen, D. X.; Wu, Z. Q.; Lee, C. J.; Harris, F. W.; Cheng, S. Z. D. *Polymer* **1993**, *34*, 3209.
31. Rojstaczer, S.; Cohn, D.; Marom, G. *J. Mater. Sci. Lett.* **1985**, *4*, 1233.